CLOSED-FORM EQUATIONS FOR DISTORTIONAL BUCKLING OF COLD-FORMED STEEL LIPPED CHANNEL COLUMNS

Daniel C. T. Cardoso

dctcardoso@puc-rio.br

Pontifícia Universidade Católica do Rio de Janeiro – PUC-Rio

Rua Marquês de São Vicente, 225, 22451-900, Rio de Janeiro, RJ, Brazil

Guilherme C. de Salles

Eduardo de M. Batista

cardoso_guilherme@poli.ufrj.br

batista@coc.ufrj.br

Universidade Federal do Rio de Janeiro – COPPE/UFRJ

Av. Horácio Macedo, 2030, 21945-972, Rio de Janeiro, RJ, Brazil

Paulo Batista Gonçalves

paulo@puc-rio.br

Pontifícia Universidade Católica do Rio de Janeiro – PUC-Rio

Rua Marquês de São Vicente, 225, 22451-900, Rio de Janeiro, RJ, Brazil

Abstract. *In this work, an energy-based approach is adopted to develop rational explicit equations for distortional buckling critical stress of lipped channel columns subject to uniform compression. Two different buckled shapes are assumed, considering i) rigid; and ii) flexible stiffened flange. To validate proposed equations, a parametric analysis is carried out for lipped channels with flange-to-web width ratio, b_f/b_w, ranging from 0.2 to 1.0 and lip-to-web width ratio, b_s/b_w, from 0.1 to 0.4. Results are compared to those obtained with generalized beam theory (GBT) for 'pure' and 'coupled' distortional modes and it is shown that, within the range of typical geometries used in industry, expressions proposed are reliable and valuable for practical design applications. Comparison is also made to benchmark methodologies, showing that proposed approaches are simpler and provide better estimates of critical loads.*

Keywords: *Distortional buckling; Thin-walled steel; Cold-formed steel; Lipped channel; Column.*

CILAMCE 2017

Proceedings of the XXXVIII Iberian Latin-American Congress on Computational Methods in Engineering P.O. Faria, R.H. Lopez, L.F.F. Miguel, W.J.S. Gomes, M. Noronha (Editores), ABMEC, Florianópolis, SC, Brazil, November 5-8, 2017.

1 INTRODUCTION

The use of cold-formed steel for main load-carrying members in structural systems has increased in the last decades, especially due to the advances in codes and standards such as the North American Specification (AISI, 2016) and the Australian/New Zealand code (AS/NZS, 2005). Analytical methods for prediction of distortional buckling critical stress are available in these codes, but they are usually complex, making their use difficult for civil engineers. Computational tools based on Finite Strip Method (e.g. CUFSM (Li and Schafer 2010), THIN-WALL-2 (Nguyen et al., 2015) and Generalized Beam Theory (e.g. GBTUL (Bebiano et al., 2008)) have also become popular to determine bifurcation loads, but engineers still prefer the use of direct formulae if available.

Distortional buckling problems are known since 1940’s and may severely affect open section thin-walled cold-formed steel members. This buckling mode is characterized by the rotation of the stiffened flange about the web-flange junction of lipped channel, hat, rack and stiffened Z sections, web flexural deformation and overall flexure (i.e. fold-line motions). Transverse plate bending of flange-stiffener assembly may also occur, although less pronounced.

Sharp (1966) is recognized as the first author to present an analytical treatment to estimate distortional buckling critical loads in lipped channel section columns, although referring to the distortional mode as “overall buckling of the lipped flange” and making certain assumptions that are not correct. Since then, many authors have dedicated efforts for a better comprehension of the phenomenon and a number of works can be found. Later, Lau and Hancock (1987) improved Sharp’s model by considering the influence of the applied stress on the web-dependent elastic restraints and allowing the flange-stiffener assembly to move laterally. The original approach allowed for prediction of distortional buckling stress of pin-ended columns with lipped channel and rack sections and non-negligible plate flexural deformations for large ratios of flange-to-web widths (b_f/b_w) were accounted by means of a correction factor. The method was rapidly accepted by the engineers and incorporated in the Australian/New Zealand standard.

To improve Lau and Hancock’s model, Schafer (1997) proposed the rotational stiffness at the web-flange junction to be expressed as the sum of elastic and stress-dependent geometric stiffness terms with contributions from flange and web. Web contribution to the rotational stiffness was obtained with finite strip method (FSM) and the new closed-form solution derived was validated with finite element method (FEM). Schafer (2000) later observed that, for members having $b_w/b_f > 4$, his model results in critical loads slightly greater than pure web buckling load, whereas Lau and Hancock’ model leads to a null load. The approach was incorporated in the recently released North American Specification.

Regarding the use of energy methods, some attempts were initially presented by Takahashi (1988), but the lack of rotation compatibility between adjacent walls remained as one of the issues of the approach. Recently, Silvestre and Camotim (2010) presented a paper with a comprehensive discussion on the distortion kinematics and mechanics for arbitrary sections and were also able to derive closed-form equations for a lipped-channel subject to compression using an energy approach. In their work, new geometric properties such as the distortional warping constant and the uniform distortion constant are introduced.

Proceedings of the XXXVIII Iberian Latin-American Congress on Computational Methods in Engineering
P.O. Faria, R.H. Lopez, L.F.F. Miguel, W.J.S. Gomes, M. Noronha (Editores), ABMEC, Florianópolis, SC, Brazil, November 5-8, 2017.

The aim of this work is to adopt an energy-based approach to derive reliable closed-form equations for lipped channels subject to uniform compression. Mechanics and kinematics of the problem are discussed and a method to determine warping stress distribution from balance of forces is presented. Two different deflected functions (models) are considered – for rigid and flexible lipped flanges – and a thorough parametric analysis is carried out for a range of geometries. Finally, results are compared to those obtained using GBT for 'pure' and 'coupled' distortional modes, as well as to benchmark methodologies currently used in design standards and specifications (Lau and Hancock, 1987, Schafer, 1997).

Throughout this paper, lipped channels are designated as b_w x b_f x b_s x t, in which b_w, b_f and b_s are web, flange and edge stiffener (or lip) widths, respectively, and t is the wall thickness, as shown in Figure 1. In the same figure, local (x, y, z) and global reference axes (X, Y, Z) are presented. The latter's origin is taken as the section centroid (C), distant Z_c from web. All calculations are performed for a half-section.

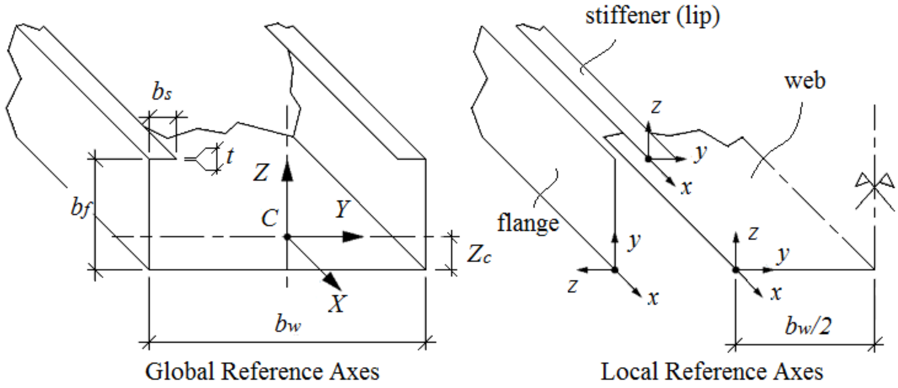

Figure 1. Cross section dimensions, local and global reference axes.

2 PROPOSED EQUATIONS

2.1 Energy equations

In the energy method adopted in this work (Rayleigh Quotient), the critical stress, σ_{crd}, is obtained from the condition of neutral equilibrium, i.e., the ratio between the strain energy, U, and the work produced by a unit uniform compressive stress, T. These quantities can be obtained as follows (e.g. Silvestre and Camotim, 2010):

$$U = \frac{E}{2}\int_{\Omega} \varepsilon^2 \mathrm{d}\Omega . \tag{1}$$

$$T = \frac{\sigma_x}{2}\int_{\Omega}\left[\left(\frac{\mathrm{d}V}{\mathrm{d}x}\right)^2 + \left(\frac{\mathrm{d}W}{\mathrm{d}x}\right)^2\right]\mathrm{d}\Omega . \tag{2}$$

Proceedings of the XXXVIII Iberian Latin-American Congress on Computational Methods in Engineering
P.O. Faria, R.H. Lopez, L.F.F. Miguel, W.J.S. Gomes, M. Noronha (Editores), ABMEC, Florianópolis, SC, Brazil, November 5-8, 2017.

in which E is the modulus of elasticity; ε is the shape-dependent strain throughout member volume, Ω; σ_x is the 'unit' applied stress profile; and V and W are the displacement components in the global directions Y and Z, respectively.

2.2 Model 1 (M1): Stiffened Flange

In Model 1, transverse flexural deformation of lipped flange is neglected and, therefore, the mode can be described as a combination of stiffened flange rotation, ϕ, bending about minor axis, δ, and web local flexure, w_w, as presented in Figure 2 and defined in Eqs. (3), (4) and (5), respectively. It can be noted that center of rotation, S, does not coincide with the web-flange junction by a distance ΔY_s and that bending about minor axis makes the rotation center move to another position (S').

$$\phi(x) = \phi_0 \sin(\pi x / L). \tag{3}$$

$$\delta(x) = \delta_0 \sin(\pi x / L) = \beta\phi_0 \sin(\pi x / L). \tag{4}$$

$$w_w(x, y) = w_{w0} f_w(y) \sin(\pi x / L) = \alpha\phi_0 f_w(y) \sin(\pi x / L). \tag{5}$$

where L is the wavelength; ϕ_0, δ_0 and w_{w0} are the amplitudes of flange-stiffener rotation, deflection to due bending and web local flexure, respectively; β and α are correlation parameters; and f_w(y) is a non-dimensional cross-sectional function for the web, which can be assumed as a 2nd order polynomial function (Eq. 6):

$$f_w(y) = (y / b_w) - (y / b_w)^2. \tag{6}$$

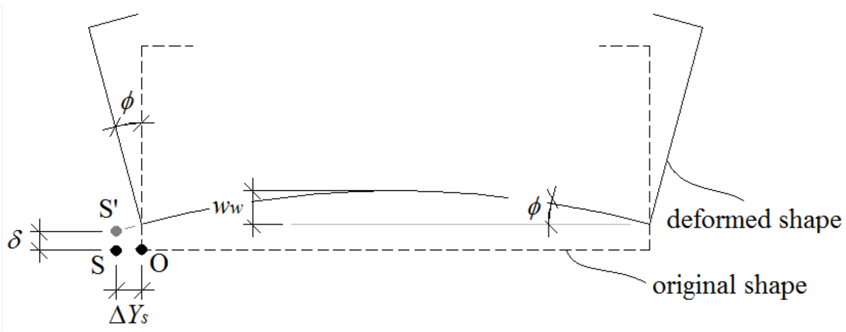

Figure 2. Motions considered for Model 1.

Coefficient α is obtained, then, from the condition of compatibility of rotation between flange and web, resulting in $\alpha = b_w$. The position of the rotation center, ΔY_s, and the coefficient β, on the other hand, can be obtained assuming balance of forces and moments about minor axis within cross-section, resulting in:

$$\Delta Y_s = \frac{b_s^{\,2}}{2b_s + b_f}. \tag{7}$$

$$\beta = \frac{b_f b_s^{\,2}(2b_f + 2b_s + b_w)}{(b_f^{\,2} + 4b_f b_s + 2b_f b_w + 6b_s b_w)(2b_s + b_f)}. \tag{8}$$

Finally, the strain energy considering the membrane and bending strain distributions resulting from assumed deflection shape and the work produced by uniform unit stress can be obtained and the final expression for the distortional buckling critical stress, $\sigma_{crd,1}$, is given as:

$$\sigma_{crd,1} = \frac{\frac{b_w D}{60}\left[\pi^2\left(\frac{b_w}{L}\right)^2 + 20 + \left(\frac{120}{\pi^2}\right)\left(\frac{L}{b_w}\right)^2\right] + \left(\beta^2\frac{\pi^2 EI_z}{L^2} + 2\beta\frac{\pi^2 EI_{zw}}{L^2} + \frac{\pi^2 EI_w}{L^2} + GJ\right)}{I_0^{\,*} + A(\Delta Y_s + \beta)^2} \tag{9}$$

in which $D = Et^3/[12(1\text{-}\nu^2)]$ is the plate bending stiffness; ν is the Poisson's ratio; G is the shear modulus; I_w is the stiffened-flange warping constant with respect to the rotation center S; I_z is the moment of inertia about minor axis (Y-Y); I_{zw} is a cross-section geometric parameter; J is the stiffened-flange Saint-Venant torsion constant; and I_0^* is an apparent polar moment of inertia with respect to point O. Geometric parameters are summarized in Table 1. Minimizing Eq. (9) with respect to L, the critical length $L_{cr,1}$ is obtained as:

$$L_{cr,1} = \sqrt[4]{\frac{\pi^4 b_w\left[Db_w^{\,3} + 60\left(EI_z\beta^2 + 2EI_{zw}\beta + EI_w\right)\right]}{120D}} \tag{10}$$

Table 1. Summary of geometric properties for a half lipped channel

Property	Expression
I_z	$\frac{b_f^{\,2}t}{6}\frac{\left(b_f^{\,2} + 4b_f b_s + 2b_f b_w + 6b_s b_w\right)}{2b_s + 2b_f + b_w}$
I_w	$\frac{b_f^{\,2}b_s^{\,3}t}{3}\frac{\left(b_f + b_s\right)^2}{\left(b_f + 2b_s\right)^2}$
I_{zw}	$-\frac{1}{6}\frac{b_f^{\,3}b_s^{\,2}t}{b_f + 2b_s}$
J (Model 1)	$\frac{t^3}{3}\left(b_s + b_f\right)$
J_s (Model 2)	$\frac{t^3}{3}b_s$
I_0^* (Model 1)	$t\left[\frac{b_s^{\,3}}{3} + \frac{b_f^{\,3}}{3} + b_s b_f^{\,2} + \frac{b_w^{\,3}}{60} + \left(\frac{b_w^{\,2}}{6} + b_s^{\,2}\right)\left(\beta + \Delta Y_s\right)\right]$
I_0^* (Model 2)	$t\left[\frac{b_w^{\,2}\kappa_1}{60}\left(b_w\kappa_1 + 10\Delta Y_s + 10\beta\right) + \kappa_2\left(\Delta Y_s + \beta\right)b_s^{\,2} + \frac{\kappa_2^{\,2}b_s^{\,3}}{3} + b_f^{\,2}b_s + \frac{\kappa_1^{\,2}b_f^{\,3}}{210b_w^{\,2}}\left(22b_f^{\,2} + 77b_f b_w + 70b_w^{\,2}\right)\right]$

2.3 Model 2 (M2): Flexible Flange

For Model 2, flange flexibility is taken into account, as shown in Figure 3. It can be seen that the web and lip rotations, θ_w and θ_s, respectively, are different from the 'overall stiffened flange rotation', ϕ. The flange flexural deformation can be defined as:

Proceedings of the XXXVIII Iberian Latin-American Congress on Computational Methods in Engineering
P.O. Faria, R.H. Lopez, L.F.F. Miguel, W.J.S. Gomes, M. Noronha (Editores), ABMEC, Florianópolis, SC, Brazil, November 5-8, 2017.

$$w_f(x,y)=\kappa_1\phi_0 y g_f(y)\sin(\pi x/L) \tag{11}$$

where κ_1 is a coefficient that correlates overall lipped flange rotation and web rotation, obtained for compatibility of rotation condition and given as:

$$\kappa_1=\frac{\theta_w}{\phi}=\frac{1}{1+\frac{2}{3}(b_f/b_w)} \tag{12}$$

and $g_f(y)$ is a non-dimensional correction function to be multiplied to the simple stiffened flange rotation function, ϕy. Assuming the flange as a frame member rotationally restrained at the web-flange junction and supported laterally at the flange-stiffener junction by a translational spring, a suitable expression for $g_f(y)$ can be obtained, as follows:

$$g_f(y)=1+(b_f/b_w)(y/b_f)-\frac{1}{3}(b_f/b_w)(y/b_f)^2 \tag{13}$$

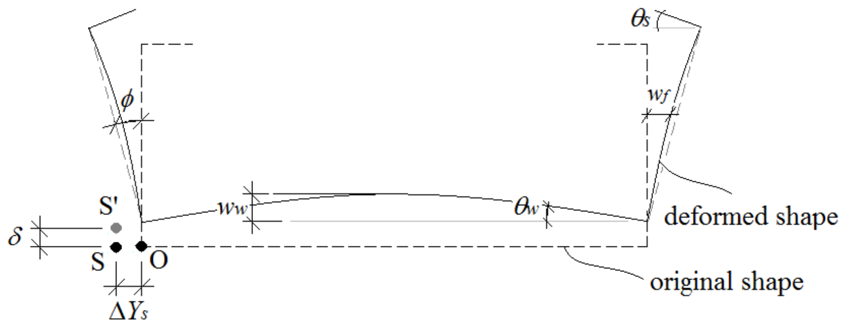

Figure 3. Motions considered for Model 2.

It is important to note that the center of rotation, S, and the bending function, δ, remain unchanged with respect to Model 1 because membrane stresses distribution is not affected by the assumption of flexible flange. However, web local flexure, w_w, and stiffener rotation, θ_s, must be redefined in order that compatibility of rotation between flange and web is preserved, as follows:

$$w_w(x,y)=b_w\kappa_1\phi_0\left[(y/b_w)-(y/b_w)^2\right]\sin(\pi x/L) \tag{14}$$

$$\theta_s(x)=\kappa_2\phi_0\sin(\pi x/L) \tag{15}$$

where coefficient κ_2 is given as:

$$\kappa_2=\frac{\theta_s}{\phi}=\frac{(b_f+b_w)}{\left[1+\frac{2}{3}(b_f/b_w)\right]b_w} \tag{16}$$

Therefore, using Rayleigh Quotient for these new deflected shapes, the closed-form equation for distortional buckling critical stress and critical length can be obtained, as follows:

Proceedings of the XXXVIII Iberian Latin-American Congress on Computational Methods in Engineering
P.O. Faria, R.H. Lopez, L.F.F. Miguel, W.J.S. Gomes, M. Noronha (Editores), ABMEC, Florianópolis, SC, Brazil, November 5-8, 2017.

$$\sigma_{crd,2} = \frac{\frac{b_w D\kappa_1^{\,2}}{60}\left[\pi^2\left(\frac{b_w}{L}\right)^2 + 20 + \left(\frac{120}{\pi^2}\right)\left(\frac{L}{b_w}\right)^2\right] + \left(\beta^2\frac{\pi^2 EI_z}{L^2} + 2\beta\frac{\pi^2 EI_{zw}}{L^2} + \frac{\pi^2 EI_w}{L^2} + \kappa_2^{\,2} GJ_s\right) + \frac{b_f D\kappa_1^{\,2}}{210}\left\{\begin{array}{l}\left[22\pi^2\left(\frac{b_f}{b_w}\right)^2 + 77\pi^2\left(\frac{b_f}{b_w}\right) + 70\pi^2\right]\left(\frac{b_f}{L}\right)^2 + \left[(224-280\nu)\left(\frac{b_f}{b_w}\right)^2 + (560-700\nu)\left(\frac{b_f}{b_w}\right) + 420(1-\nu)\right] + \\ \frac{280}{\pi^2}\left(\frac{b_f}{b_w}\right)^2\left(\frac{L}{b_f}\right)^2\end{array}\right\}}{I_0^{\,*} + A(\Delta Y_s + \beta)^2} \tag{17}$$

$$L_{cr,2} = \sqrt[4]{\frac{\pi^4\kappa_1}{840 b_w}\left[44 b_f^{\,5} + 154 b_f^{\,4} b_w + 140 b_f^{\,3} b_w^{\,2} + 7 b_w^{\,5} + \frac{420}{D}(b_w/\kappa_1)^2\left(EI_z\beta^2 + 2EI_{zw}\beta + EI_w\right)\right]} \tag{18}$$

where $J_s = b_s t^3/3$ is the lip constant of torsion. The other geometric properties are presented in Table 1.

3 COMPARISON WITH GBT AND OTHER METHODOLOGIES

To evaluate the accuracy of proposed equations, a comparison with Generalized Beam Theory (Schardt, 1994) is carried out. For this purpose, a GBT-based software developed at IST-Lisbon, GBTUL (Bebiano et al., 2008) is adopted. For all analyzes performed, E = 200 GPa and ν = 0.3 were considered.

Sections having b_w = 100 mm and t = 1 mm with b_f/b_w and b_s/b_w ranging respectively from 0.2 to 1.0 and 0.1 to 0.4 are initially considered. Initially, pure distortional mode with single curvature (Silvestre and Camotim, 2010) is considered. In all, thirty six different geometries were considered and the relative differences are presented in Table 2 along with section ID. It can be seen that M1 resulted in greater differences for sections having larger b_f/b_w and b_s/b_w ratios, whereas M2 resulted in almost 'exact' results. Cross-section geometries within the range of typical lipped channel sizes obtained from standards and company brochures are highlighted in Table 2. Maximum relative differences are 1.180 for M1 and 0.993 for M2 within the range of applicable sections, while average differences are 1.056±0.081 and 0.997±0.002, respectively.

Table 2. Section ID (#) and Relative differences between Models 1 and 2 and GBTUL for pure distortional mode (σ_{crd} / $\sigma_{\text{crd,GBT}}$).

b_s/b_w ↓	Model 1								
0.4	1.032 (#36)	1.059 (#32)	1.086 (#28)	1.110 (#24)	1.133 (#20)	1.154 (#16)	1.173 (#12)	1.191 (#8)	1.208 (#4)
0.3	1.000 (#35)	1.022 (#31)	1.047 (#27)	1.075 (#23)	1.099 (#19)	1.122 (#15)	1.143 (#11)	1.163 (#7)	1.180 (#3)
0.2	0.957 (#34)	0.975 (#30)	1.005 (#26)	1.034 (#22)	1.065 (#18)	1.091 (#14)	1.112 (#10)	1.134 (#6)	1.149 (#2)
0.1	0.908 (#33)	0.924 (#29)	0.959 (#25)	0.996 (#21)	1.028 (#17)	1.054 (#13)	1.076 (#9)	1.094 (#5)	1.110 (#1)
b_f/b_w →	0.2	0.3	0.4	0.5	0.6	0.7	0.8	0.9	1.0
b_s/b_w ↓	Model 2								
0.4	0.992	0.996	0.998	0.999	0.999	0.999	0.999	0.999	0.998

Proceedings of the XXXVIII Iberian Latin-American Congress on Computational Methods in Engineering
P.O. Faria, R.H. Lopez, L.F.F. Miguel, W.J.S. Gomes, M. Noronha (Editores), ABMEC, Florianópolis, SC, Brazil, November 5-8, 2017.

0.3	0.992	0.996	0.997	0.996	0.998	0.999	0.998	0.999	0.997
0.2	0.993	0.996	0.996	0.998	0.998	0.998	0.999	0.999	0.999
0.1	0.993	0.996	0.997	0.998	0.998	0.998	0.999	0.999	0.999
$b_f/b_w \rightarrow$	0.2	0.3	0.4	0.5	0.6	0.7	0.8	0.9	1.0

* highlighted region: geometries within the range of typical lipped channel sizes.

To evaluate the influence of linear coupling of distortion (Φ_d) with other functions such as local (Φ_ℓ) and global (Φ_g), comparison was carried out again with those obtained using the software GBTul, only this time with all deformation modes activated. In Figure 4, ratio between critical stresses obtained with GBTul for pure distortional mode and for all modes activated ($\sigma_{crd,GBT}/\sigma_{cr,GBT}$) are plotted in a b_s/b_w x b_f/b_w map. The map is also divided into 3 regions according to the participation of each individual shape into the final buckling mode: D = pure distortion (Φ_d > 90%); D+G = coupling between distortion and global (Φ_g > 10-50%; negligible Φ_ℓ); D+L = coupling between distortion and local (Φ_ℓ > 10-30%; negligible Φ_g). The following comments can be made: i) influence of local or global functions increases with b_s/b_w and reduces with b_f/b_w; ii) sections having low b_f/b_w and b_s/b_w ratios have a greater participation of local mode; iii) global deformation mode plays a major role for lower b_f/b_w and larger b_s/b_w ratios; iv) influence of local shape is more pronounced in columns having closer distortional and local individual critical lengths; and iv) linear coupling is negligible for most sections within commercially-available domain Λ. It is important to mention that similar results can be obtained using FSM.

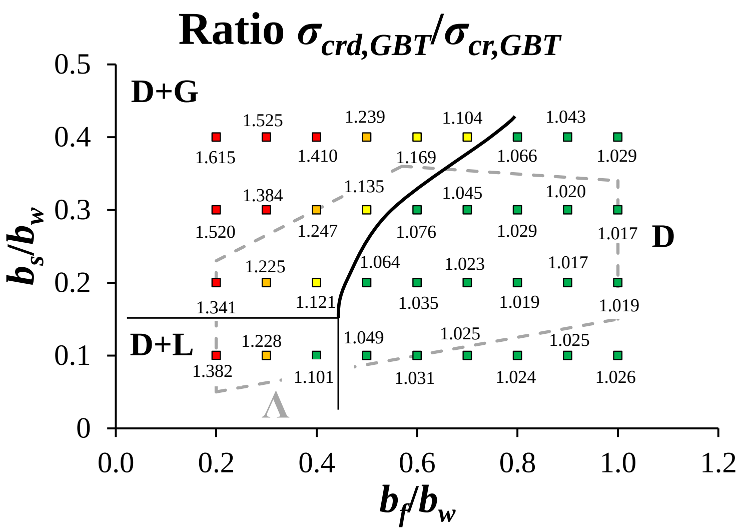

Figure 4. Ratio between critical stresses obtained using GBTul with pure distortional mode ($\sigma_{crd,GBT}$) and all deformation modes activated ($\sigma_{cr,GBT}$), presented in a b_s/b_w x b_f/b_w 'map'.

Finally, results obtained with proposed equations are compared to those obtained using methods presented by Lau and Hancock (1987) and Schafer (1997), which are benchmarks methodologies recommended in the Australian/New Zealand standard (AS/NZS, 2005) and North American Specification (AISI, 2016), respectively. In Figure 5, ratios between critical stresses obtained using different analytical methods and GBTUL with all modes activated ($\sigma_{crd}/\sigma_{cr,GBT}$) are plotted for cross-sections within Λ domain. It can be seen that all methods provide good estimate of critical loads for sections having $b_f/b_w \geq 0.4$ (up to #26), with a better agreement being achieved for Model 2. The estimates deviate from the averages regardless the method used for sections having $b_f/b_w < 0.4$, which may be explained by the linear coupling effect described previously. It is also important to note that the Model 1 equation resulted in a level of accuracy similar to Schafer's approach (1997), but with much less calculation effort, whereas, in comparison, Lau and Hancock's approach (1987) provided slightly better estimates within the range of sections investigated.

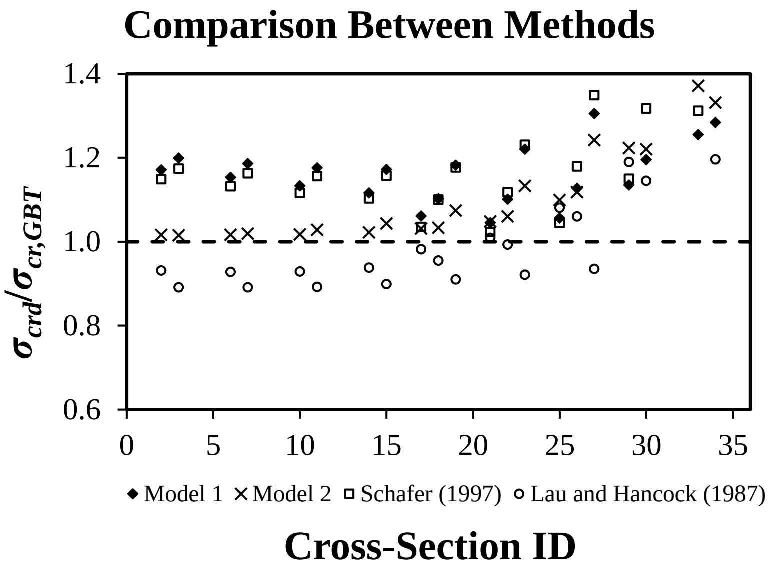

Figure 5. Comparisons for different approaches with respect to GBTUL with all deformation modes activated, for sections within Λ.

4 CONCLUSIONS

In this work, the development of closed-form equations for predicting distortional buckling critical stress was presented. A parametric analysis was carried out and it was shown that average differences with respect to pure distortional buckling stresses using with GBTUL were 1.056±0.081 and 0.997±0.002 for M1 and M2, respectively. It can be concluded that M1 resulted in a simpler but less accurate equation, whereas equation derived from M2 is more complex and difficult to be implemented, but very accurate.

It is important to mention that some cross-sections considered to define region Λ are usually not recommended for practical applications. For instance, sections having $b_f/b_w < 0.3$ usually exhibit very low global buckling critical loads, whereas sections having $b_f/b_w > 0.8$ and $b_s/b_w < 0.1$ are not effective against distortional buckling, i.e., resulting in lower critical loads, as can be seen in Table 3. If these practical limits are imposed to define the bounds of the region of interest, results for Model 1 within Λ would be greatly improved.

Comparison was also made to the results obtained considering linear coupling between distortion, local and global deflected shapes. It is shown that this interaction affects the behavior and reduces significantly the critical loads, especially for sections having lower b_f/b_w and greater b_s/b_w ratios. Proposed equations were also compared to methodologies recommended in the Australian/Neo Zealand standard (XX) and North American specification (XX) and to critical stresses obtained with GBTul considering all deformation modes activated, for sections within Λ. It was shown that all methods deviated significantly from their average differences when b_f/b_w reduces (< 0.4), which can be explained by the linear coupling effect. M2 provided a superior agreement among compared methods for $b_f/b_w \geq 0.4$ whereas levels of accuracy were similar for M1 and Schafer's approach (XX).

ACKNOWLEDGEMENTS

The authors would like to thank the support of Brazilian research agencies CAPES, CNPq and FAPERJ.

REFERENCES

AISI (American Iron and Steel Institute), 2016. North American Specification (NAS) for the design of cold-formed steel structural members – AISI S100-16-C, Washington, DC.

AS-NZS (Standards of Australia and Standards of New Zealand), 2005. Australian/New Zealand Standard on Cold-Formed Steel Structures - AS/NZS 4600, 2nd ed., Sydney, Wellington.

Bebiano R., Pina P., Silvestre N., Camotim D., 2008. GBTUL1.0b - buckling and vibration analysis of thin-walled members. Technical University of Lisbon.

Lau S., Hancock G., 1987. Distortional buckling formulae for channel columns. *ASCE Journal of Structural Engineering*, vol. 113, n. 5, pp. 1063-78.

Li Z., Schafer B.W., 2010. Buckling analysis of cold-formed steel members with general boundary conditions using CUFSM: conventional and constrained finite strip methods. *Proc. of the 20th International Spec. Conf. on Cold-Formed Steel Structures,* St. Louis, MO, USA, November.

Nguyen, V.V., Hancock, G.J., Pham, C.H., 2015. Development of the THIN-WALL-2 program for buckling analysis of thin-walled sections under generalised loading. *Proc. of the 8th International Conf. on Advances in Steel Structures*, Lisbon, Portugal.

Schafer B.W.,1997. Cold-formed steel behaviour and design: analytical and numerical modeling of elements and members with longitudinal stiffeners. PhD Thesis, Cornell University/USA.

Schafer B.W., 2000. Distortional buckling of cold-formed steel columns. Final Report, Project sponsored by The American Iron and Steel Institute, Washington, DC.

Schardt R., 1994. Generalized beam theory – an adequate method for coupled stability problems. *Thin-Walled Structures*, vol. 19, n. 2-4, pp. 161-180.

Sharp M.L., 1966. Longitudinal stiffeners for compression members. *ASCE Journal of the Structural Division*, vol. 92, n. 5, pp. 187-211.

Silvestre N., Camotim D., 2010. On the mechanics of distortion in thin-walled open sections. *Thin-Walled Structures*, vol. 48, n. 7, pp. 469-481.

Takahashi, K., 1988. A new buckling mode of thin-walled open cross section members. *Applied Solid Mechanics-2*, vol. 25, pp. 553-573.